Measurement of the biaxial permittivities for several smectic C host materials used in ferroelectric liquid crystal devices

J. C. Jones[a]; E. P. Raynes[a]

[a] Electronics Division of the Defence Research Agency, Malvern, Worcestershire, England

PLEASE SCROLL DOWN FOR ARTICLE

Measurement of the biaxial permittivities for several smectic C host materials used in ferroelectric liquid crystal devices

by J. C. JONES* and E. P. RAYNES

Electronics Division of the Defence Research Agency, RSRE Malvern,
St. Andrews Road, Malvern, Worcestershire WR14 3PS, England

Dielectric biaxiality plays an important role in the electric field behaviour of ferroelectric liquid crystal devices, providing the necessary driving force for AC field stabilization and playing an important role in device dynamics. The static electric permittivities have been measured as a function of temperature for several mixtures with an N–S_A–S_C phase sequence. Three permittivities are defined for the biaxial S_C phase, and were determined from measurements of homeotropic and planar cells and from the average permittivity $\bar{\varepsilon}$ extrapolated from the uniaxial nematic and smectic A phases. The S_C cone angle is assumed to be equivalent at dielectric and optical frequencies. Results are reported for five common ferroelectric liquid crystal hosts and for two racemic mixtures, including the racemic analogue of the commercially available SCE13. The dielectric biaxiality is sufficiently large below the S_A to S_C transition in each of the studied mixtures to have a strong influence on the electro-optic behaviour. This is consistent with the occurrence of AC stabilization in surface stabilized ferroelectric liquid crystal devices with the chevron layer configuration.

1. Introduction

Although the electro-optic properties of surface stabilized ferroelectric liquid crystal devices are usually dominated by the spontaneous polarization, the electric permittivities can also play an important role. At high field strengths, the device switching time deviates from a reciprocal relationship with applied field due to the effect of the permittivities [1]. This often leads to a minimum switching time which has important implications for the multiplexed operation of the surface stabilized ferroelectric device [2, 3]. Another consequence of ferroelectric liquid crystal dielectric behaviour is AC field stabilization of the fully switched states, which is often used to maintain optimum optical bistability of the device [4]. Recently, it has been demonstrated that AC field stabilization requires that the S_C^* possesses a significant dielectric biaxiality [5] for ferroelectric devices in which the smectic layers are arranged in a chevron configuration [6]. It is also shown in [5] that a negative dielectric anisotropy is actually detrimental to the AC field effect. However, many materials with large negative $\Delta\varepsilon$ exhibit AC field stabilization and therefore such materials must be strongly biaxial. Thus, accurate measurements of the three S_C^* permittivities are essential for the full understanding of ferroelectric liquid crystal electric field behaviour and the optimization of the materials for use in devices.

Refractive index measurements [7] showed that the S_C^* optical biaxiality is negligible, which has often led to the assumption that ferroelectric liquid crystals are

* Author for correspondence.

uniaxial even at audio frequencies. Techniques for measuring the biaxial permittivities of S_C [8] and S_C^* [9] samples have been reported, but the director and layer configurations in those reports are uncertain, leading to doubts concerning the accuracy of those results. Accurate permittivity measurements require uniform samples in which the director profile is known. For materials with an $N^{(*)}$–S_A–$S_C^{(*)}$ phase sequence, there are two cell geometries for which the $S_C^{(*)}$ layer geometry is well understood: based on homeotropic and planar surface alignments. With homeotropic alignment, the smectic layers are parallel to the cell plane and the director precesses about the layer normal to form the characteristic schlieren texture when viewed between crossed polarizers [10]. Low tilt, planar alignment leads to a chevron layer structure in which the smectic layer normal is tilted from the cell plane by $+\delta$ at one surface and $-\delta$ at the other. At the chevron interface, the director is constrained to be parallel to the surfaces with an in-plane twist angle β_i away from the alignment direction

$$\cos \beta_i = \cos \theta / \cos \delta. \tag{1}$$

The ratio of $S_C^{(*)}$ layer tilt and cone angles (δ/θ) is independent of temperature and usually about 0·9. Thus, β_i is substantially lower than the cone angle in the surface-stabilized state, which is typically about 10°. Microscopic studies show that the sample is divided into domains for which best extinction of white light occurs on opposite sides of the alignment direction, corresponding to director orientations on opposite sides of the cone. Optical measurements [11] suggest that the director profile is approximately uniform within each domain: the director has an in-plane twist β_i but little out-of-plane tilt, as shown in figure 1 (a). More recent work shows that the surface stabilized state is more accurately modelled by a triangular director profile [12], figure 1 (b), and this is used to explain the coloration of the ferroelectric liquid crystal domain at the condition
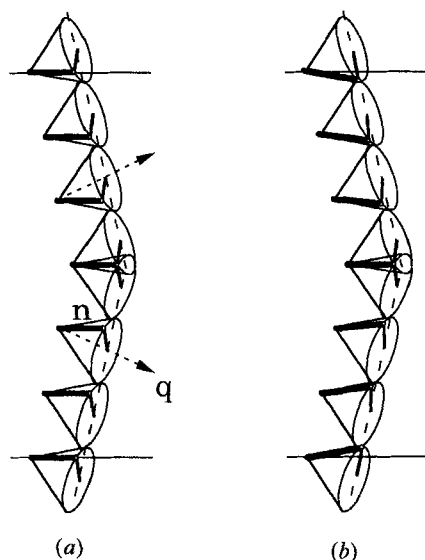

Figure 1.   Two possible planar director profiles based on the chevron layer structure:
(a) uniform and (b) triangular director profiles.

for best extinction. The difference in the measured permittivities in the planar geometry with a uniform director profile and a triangular profile is discussed in section 4, where it is shown that a uniform director profile is an acceptable approximation.

2. The S_C coordinate geometry and permittivities

A generalized $S_C^{(*)}$ geometry is shown in figure 2, in which the director **n** has the frame of reference (1, 2, 3) and the laboratory (x, y, z). The director is tilted from the layer normal **q** by the cone angle θ, the position of the director around the cone of possible orientations is described by an azimuthal angle φ, and the layer normal is tilted by an angle δ. These angles specify right handed rotations about the 2 direction, 3 direction and 1 direction, respectively, and may be expressed as matrices $\mathbf{R}_\theta$, $\mathbf{R}_\varphi$ and $\mathbf{R}_\delta$. The $S_C^{(*)}$ material properties determined in the laboratory reference frame may be related to the director reference frame using the rotation $\mathbf{R}$

$$\mathbf{R} = (\mathbf{R}_\delta) \quad (\mathbf{R}_\varphi) \quad (\mathbf{R}_\theta). \tag{2}$$

Thus, in the laboratory frame of reference the **n** director has components

$$\begin{pmatrix} n_x \\ n_y \\ n_z \end{pmatrix} = \mathbf{R} \begin{pmatrix} 0 \\ 0 \\ 1 \end{pmatrix} = \begin{pmatrix} \cos \varphi \sin \theta \\ \cos \delta \sin \varphi \sin \theta - \sin \delta \cos \theta \\ \sin \delta \sin \varphi \sin \theta + \cos \delta \cos \theta \end{pmatrix}. \tag{3}$$

Similarly, the permittivity in the laboratory frame of reference ε' is related to the permittivity in the director frame ε through

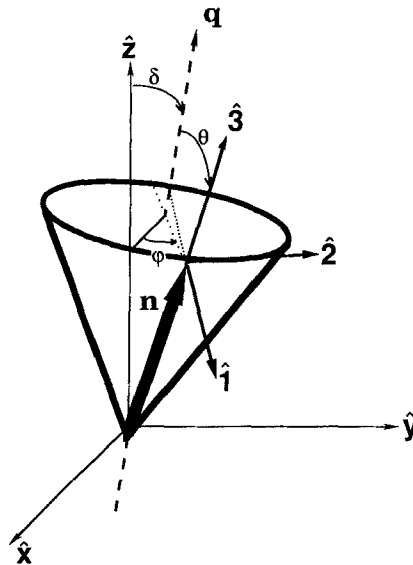$$\varepsilon' = \mathbf{R} \varepsilon \tilde{\mathbf{R}}, \tag{4}$$

Figure 2. S_C coordinate geometry and the relationship between the director (1, 2, 3) and laboratory (x, y, z) frames of reference.

where

$$\varepsilon = \begin{pmatrix} \varepsilon_1 & 0 & 0 \\ 0 & \varepsilon_2 & 0 \\ 0 & 0 & \varepsilon_3 \end{pmatrix}. \tag{5}$$

The components of the permittivity tensor in the laboratory frame ε' are then

$$\varepsilon_{xx} = \varepsilon_1 \cos^2 \varphi \cos^2 \theta + \varepsilon_2 \sin^2 \varphi + \varepsilon_3 \cos^2 \varphi \sin^2 \theta,$$

$$\varepsilon_{xy} = \varepsilon_{yx} = \varepsilon_1 \cos \varphi \cos \theta (\cos \delta \sin \varphi \cos \theta + \sin \delta \sin \theta)$$

$$- \varepsilon_2 \cos \delta \cos \varphi \sin \varphi + \varepsilon_3 \cos \varphi \sin \theta (\cos \delta \sin \varphi \sin \theta - \sin \delta \cos \theta),$$

$$\varepsilon_{xz} = \varepsilon_{zx} = \varepsilon_1 \cos\varphi \cos \theta (\sin \delta \sin \varphi \cos \theta - \cos \delta \sin \theta)$$

$$- \varepsilon_2 \sin \delta \cos \varphi \sin \varphi + \varepsilon_3 \cos \varphi \sin \theta (\sin \delta \sin \varphi \sin \theta + \cos \delta \cos \theta),$$

$$\varepsilon_{yy} = \varepsilon_1 (\cos \delta \sin \varphi \cos \theta + \sin \delta \sin \theta)^2 + \varepsilon_2 \cos^2 \delta \cos^2 \varphi + \varepsilon_3 (\cos \delta \sin \varphi - \sin \delta \cos \theta)^2,$$

$$\varepsilon_{yz} = \varepsilon_{zy} = \varepsilon_1 (\cos \delta \sin \varphi \cos \theta + \sin \delta \sin \theta)(\sin \delta \sin \varphi \cos \theta - \cos \delta \sin \theta)$$

$$+ \varepsilon_2 \sin \delta \cos \delta \cos^2 \varphi + \varepsilon_3 (\cos \delta \sin \varphi \sin \theta$$

$$- \sin \delta \cos \theta)(\sin \delta \sin \varphi \sin \theta + \cos \delta \cos \theta),$$

$$\varepsilon_{zz} = \varepsilon_1 (\sin \delta \sin \varphi \cos \theta - \cos \delta \sin \theta)^2 + \varepsilon_2 \sin^2 \delta \cos^2 \varphi$$

$$+ \varepsilon_3 (\sin \delta \sin \varphi \sin \theta + \cos \delta \cos \theta)^2. \tag{6}$$

In practice, the laboratory frame is defined by the glass cell which contains the liquid crystal.

Caution is required when discussing the reference frame (1, 2, 3). The symmetry of the S_C phase is limited to a mirror plane and a two-fold rotation axis perpendicular to the plane containing the nematic-like n-director and layer normal. This direction, denoted 2 in figure 2, provides the only well-defined principal axis of the S_C and S_C^* systems, indeed it represents the direction of the ferroelectric polarization in an S_C^*. Thus, directions 1 and 3 may have any orientation θ about the 2 axis, which may also vary with frequency, and the dielectric director n and cone angle θ are not necessarily equivalent to the optical n and θ. However, cone angles determined from permittivity measurements compare well with those measured in optical [8] and X-ray studies [13], and so the optic and dielectric cone angles are assumed to be equivalent for the present work.

To aid visualization, it is convenient to represent the director orientation by the degree of tilt out of the cell plane ζ, and twist β away from the preferred alignment direction but parallel to the cell walls (see figure 3). The terms tilt and twist are used to denote director orientation and neither implies any distortion of the director field. If the director profile is uniform, β is equivalent to the angle between the optic axis and the preferred alignment direction or extinction angle. With planar alignment and an S_A phase immediately above the $S_C^{(*)}$, as normally used in the ferroelectric liquid crystal device, the surface normal is parallel to the y direction and the preferred alignment direction in the planar geometry is the z axis. The layer normal and z direction are equivalent in the S_A planar geometry but cooling to an $S_C^{(*)}$ causes tilt of the layer normal with respect to the z axis through an angle δ. The in-plane twist β is then defined
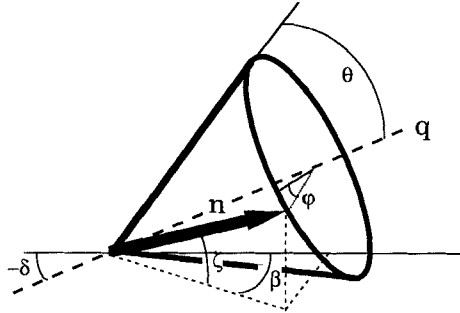
Figure 3. Definition of the director out-of-plane tilt angle ζ and the in-plane twist angle β in the laboratory reference frame.

as the angle between the z axis and the component of the director in the xz plane, which is found from equation (3)

$$\tan \beta = \frac{\cos \varphi \sin \theta}{\sin \delta \sin \varphi \sin \theta + \cos \delta \cos \theta}. \tag{7}$$

Similarly, the out-of-plane tilt ζ is

$$\sin \zeta = \cos \delta \sin \varphi \sin \theta - \sin \delta \cos \theta. \tag{8}$$

Figure 4 shows β and ζ as a function of the azimuthal angle φ for typical values of $\theta = 22 \cdot 5°$ and $\delta = 19°$. In a ferroelectric S_C^*, application of a DC electric field couples to the spontaneous polarization and causes a change of azimuthal angle towards $\varphi = n\pi$ ($n = 0, 1, 2, \ldots$). Substituting $\varphi = n\pi$ into equation (7) leads to an expression for the in-plane twist angle of the fully switched state β_s

$$\tan \beta_s = \tan \theta / \cos \delta \tag{9}$$

and the fully switched out-of-plane tilt angle ζ_s from equation (8)

$$\sin \zeta_s = -\sin \delta \cos \theta. \tag{10}$$

In a planar aligned cell with symmetric chevron layers, director continuity across the chevron interface restricts the director to the xz plane ($\zeta = 0$) at the cell centre [14]. The azimuthal angle at the interface φ_i is then given by

$$\sin \varphi_i = \tan \delta / \tan \theta, \tag{11}$$

which on substitution into equation (7) yields equation (1).

With the electric field applied parallel to the y direction of the laboratory frame, the measured permittivity ε is ε_{yy}, which may be rewritten in the form

$$\varepsilon = \varepsilon_1 + \Delta\varepsilon \sin^2 \zeta + \partial\varepsilon \cos^2 \delta \cos^2 \varphi, \tag{12}$$

where the two $S_C^{(*)}$ dielectric anisotropies are defined as $\Delta\varepsilon = (\varepsilon_3 - \varepsilon_1)$ and $\partial\varepsilon = (\varepsilon_2 - \varepsilon_1)$. In the homeotropic geometry, $\delta = \pi/2$ and the measured permittivity ε_h is

$$\varepsilon_h = \varepsilon_1 + \Delta\varepsilon \cos^2 \theta. \tag{13}$$

This is equivalent to ε_{zz} with $\delta = 0$. With well oriented homeotropic layers, this equation will apply even where the director varies throughout the sample. For the planar
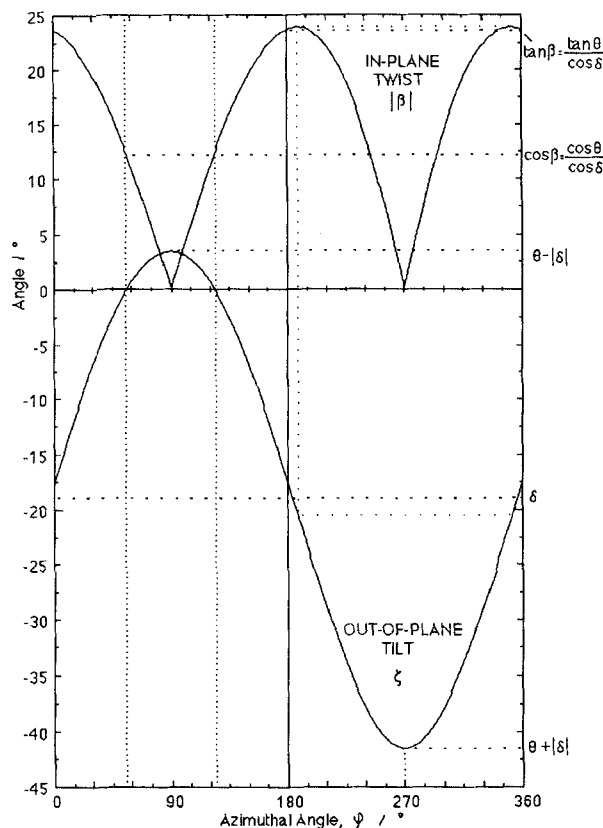
Figure 4. Out-of-plane tilt ζ and in-plane twist β of the director as a function of azimuthal angle φ for typical values of $\theta = 22\cdot5°$ and $\delta = 19°$.

geometry with a uniform director profile $\zeta = 0$ and substitution of equation (11) into equation (12) leads to

$$\varepsilon_{\rm p} = \varepsilon_2 - \partial\varepsilon \frac{\sin^2 \delta}{\sin^2 \theta}. \tag{14}$$

With typical chevron cells, the layer tilt angle is nearly equal to the cone angle and the largest contribution to the measured permittivity is from ε_1. The permittivity for non-uniform samples is derived in §4.

3. Experimental

The practical approach of developing ferroelectric liquid crystal mixtures suitable for application is to dope an achiral S_C host with a chiral dopant to induce ferroelectricity [15]. Properties such as the phase sequence and transition temperatures, and many of the material parameters, such as the permittivities, refractive indices and S_C^* cone angle, are largely determined by the host because the dopant is usually a small proportion of the mixture. Permittivity measurements for achiral S_C mixtures used as hosts in commercial ferroelectric liquid crystals are reported here to avoid problems associated with the chirality and ferroelectricity of the doped mixtures, such as the formation of half-splayed states [16]. Results for racemic analogues of two ferroelectric liquid crystal mixtures including the commercially available SCE13 are

also reported. Any differences in the physical properties of the chiral and racemic forms of a mixture are expected to be negligible and the nomenclature $S_C^{(*)}$ is used to indicate either form.

Host systems based on the fluoro-phenyl-biphenyl-carboxylates (MBF) [17], phenylpyrimidines (PYP) [18] mono-fluoroterphenyls (FTP) [19] and di-fluoroterphenyls (DiFTP) [20] were studied, the chemical structure for which are shown in table 1. Also measured was a DiFTP host in a mixture with a racemic transverse cyano-dopant [21] and the racemic analogue of SCE13. Each mixture used was designed to exhibit an N–S_A–S_C phase sequence and the composition and transition temperatures are listed in table 2. Permittivities were determined from capacitance measurements made using an impedance analyser (HP4192A) at the frequency 100 Hz and with 1 V_{rms}. Homeotropic and planar alignment geometries were defined using chrome-complex and 30° evaporated SiO alignment layers, respectively.

Table 1. Chemical structure of the liquid crystal materials.
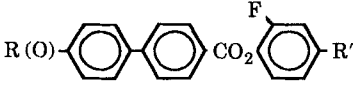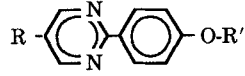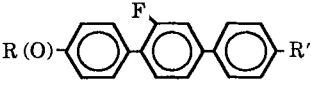
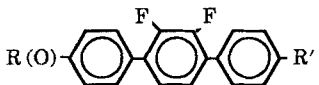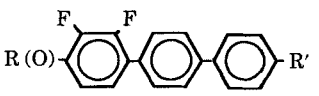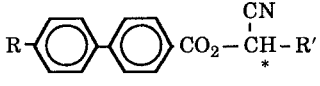| Structure	Acronym	Reference
R(O)—◯—◯—CO₂—◯—R′ (F)	MBF	[17]
R—◯(N)—◯—O-R′	PYP	[18]
R(O)—◯—◯—◯—R′ (F)	FTP	[19]
R(O)—◯—◯—◯—R′ (F F)	DI-FTP 1	[20]
R(O)—◯—◯—◯—R′ (F F)	DI-FTP 2	[20]
R—◯—◯—CO₂—CH(CN)—R′	CYANO-dopant	[21]

Table 2. Host mixture compositions and phase transition temperatures.

Host	Composition wt.%	Transition temperatures/°C					
		I	N	S_A	S_C	$S_?$ †	C
H1	MBF 8.5 (66·7) MBF 7.5 (33·3)	138·0	82·7	73·3	(32·0)	{B}	59
H2	MBF 8.5 (33·3) MBF 8O.5 (33·3) MBF 7O.7 (33·3)	151·7	112·7	107·3	27·8	{B}	<−20
H3	PYP 9O.9 (66·7) PYP 7O.9 (33·3)	71·8	70·0	55·0	—		23·2
H4	FTP 9.3 (72·1) FTP 8O.3 (27·9)	131·2	80·1	66·8	(29·0)	{B}	48·8
H5	DiFTP 1 5.5 (33·3) DiFTP 1 7.5 (33·3) DiFTP 2 5.5 (33·3)	127·0	97·2	91·5	(20·0)	{?}	38·0
M1	DiFTP 1 7.5 (46.25) DiFTP 2 5.5 (23·125) DiFTP 2 7.5 (23·125) Racemic dopant (7.5)	113·9	102·8	62·8			
SCE13(R)	BDH mixture	100·8	86·3	60·8	<−20	{I}	

† Underlying smectic phases are bracketed where known.

The cell spacing used was nominally $4\,\mu$m. Accuracies of better than 0·25 per cent were achieved for the I and N permittivities using a robust cell design with guarded electrodes [22].

In each mixture, the homeotropic permittivity ε_h tends towards the mean permittivity $\bar\varepsilon$ on cooling below the S_A–S_C phase transition because of tilting of the director through the cone angle θ, as implied by equation (13). Also, the gradient of the planar permittivity ε_p with temperature, $|d\varepsilon_p/dT|$, lowered on cooling through the S_A–S_C transition for each material. For the hosts with negative dielectric anisotropy, this decrease could be interpreted using an average out-of-plane tilt of across the sample volume which is typically $25° \pm 5°$. This interpretation, however, contradicts the evidence from optical experiments and it cannot be used for the positive $\Delta\varepsilon$ PYP host where any out-of-plane tilt would lead to an increase in $|d\varepsilon_p/dT|$. Instead, we interpret the decrease of $|d\varepsilon_p/dT|$ at the S_A to S_C transition as a result of the finite dielectric biaxiality and the appearance of the chevron structure with no significant out-of-plane tilt: the measured planar permittivity in the $S_C^{(*)}$ phase is then approximately ε_1, the lesser of the two perpendicular permittivities, whereas the measured permittivity in the S_A phase is $(\varepsilon_1 + \varepsilon_2)/2$.

Layer tilt and cone angles δ and θ were determined using a novel method based on optical critical angle measurements [23]. The temperature dependence of the cone angle was fitted to

$$\theta = \theta_0(T_{S_CS_A} - T)^\gamma. \tag{15}$$

Values for θ_0 and γ are listed in table 3, together with the temperature independent constant δ/θ, for each mixture. The θ_0, γ and δ/θ values for H2 and M1 were assumed to be equivalent to the similar mixtures, H1 and H5, respectively.

Determination of the three $S_C^{(*)}$ permittivities, however, requires a third permittivity measurement. The mean $S_C^{(*)}$ permittivity $\bar\varepsilon$ is given by

$$\bar\varepsilon = (\varepsilon_1 + \varepsilon_2 + \varepsilon_3)/3, \tag{16}$$

where $\varepsilon_{\parallel} = \varepsilon_3$ and $\varepsilon_{\perp} = \varepsilon_1 = \varepsilon_2$ in the uniaxial nematic and smectic A phases. A linear extrapolation of the temperature dependence from the uniaxial phases was used to determine $\bar\varepsilon$ in the S_C phase and ε_1, ε_2 and ε_3 were found by solving equations (13), (14) and (16). The temperature dependence of the measured permittivities ε_h and ε_p, the extrapolation of $\bar\varepsilon$ and the calculated S_C permittivities for each of the materials studied are plotted in figures 5 to 11, and the results summarized in table 4 for the shifted temperature $T_{S_CS_A} - T = 30°$C. The dielectric biaxiality values for the MBF hosts H1 and H2 are similar to that inferred from a comparison of the high frequency AC and the DC electric field effects in the commercial FLC SCE3 [25], which is also based on an MBF host.

Table 3. Fitting parameters for the host cone and layer tilt angles.

Host	$T_C/°$C $\pm$0·5	$\theta_0/°$ $\pm$0·3	γ $\pm$0·02	δ/θ $\pm$0·05
H1 (MBF)	73·3	4·0	0·46	0·91
H3(PYP)	55·0	6·2	0·33	0·90
H4 (FTP)	66·8	7·4	0·31	0·88
H5 (DiFTP)	91·5	4·2	0·44	0·87
SCE13(R)	60·8	5·0	0·40	0·90

Figure 5. Temperature dependence of the permittivities for the di-alkyl MBF host H1.

Figure 6. Temperature dependence of the permittivities for the alkyl-alkoxy MBF host H2.

Figure 7. Temperature dependence of the permittivities for the PYP host H3 [24].

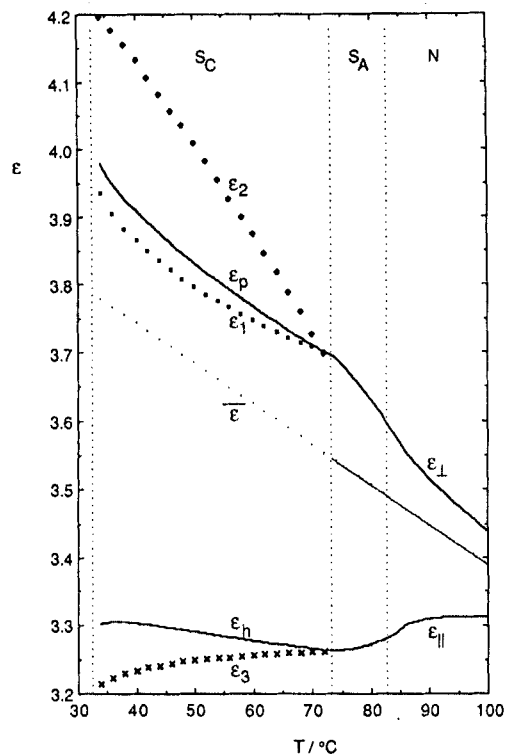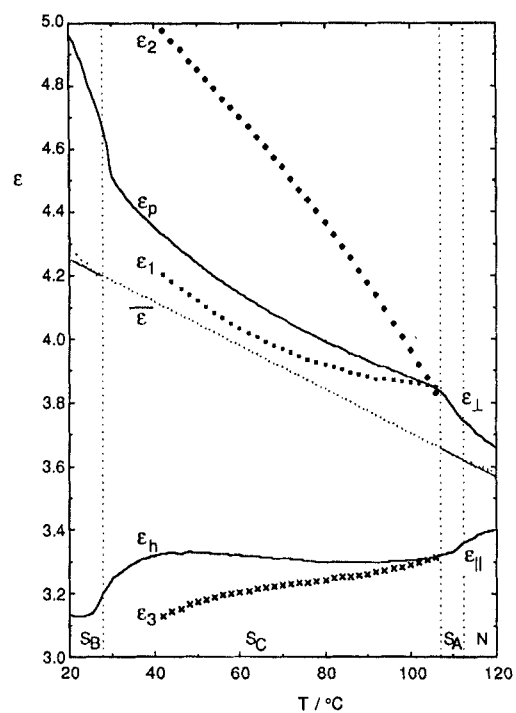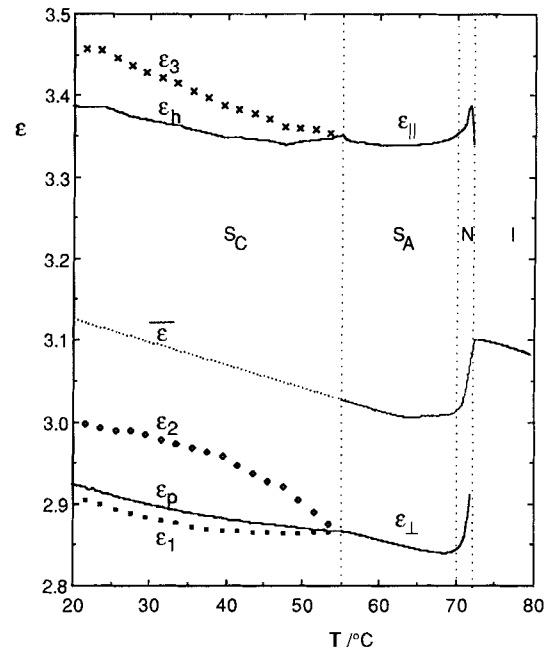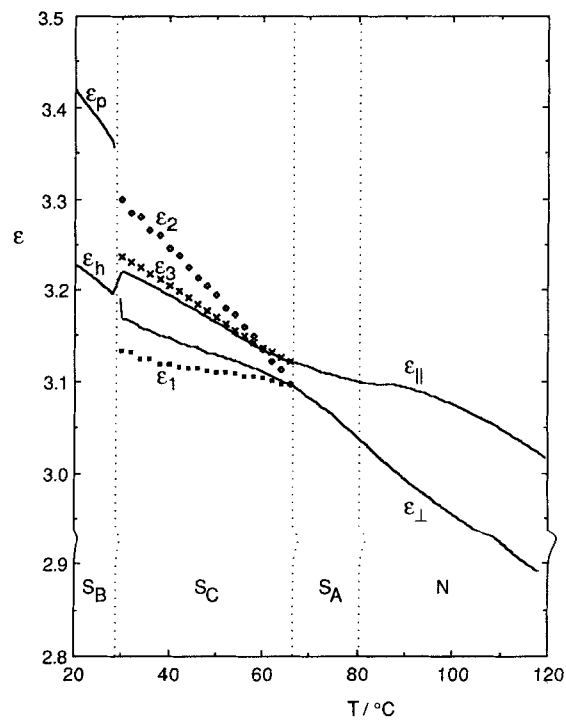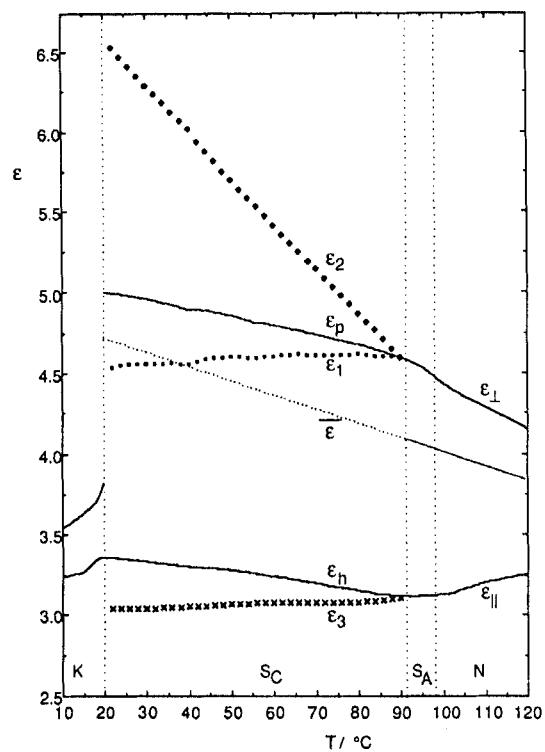Figure 8. Temperature dependence of the permittivities for the FTP host H4.

Figure 9. Temperature dependence of the permittivities for the DiFTP host H5.
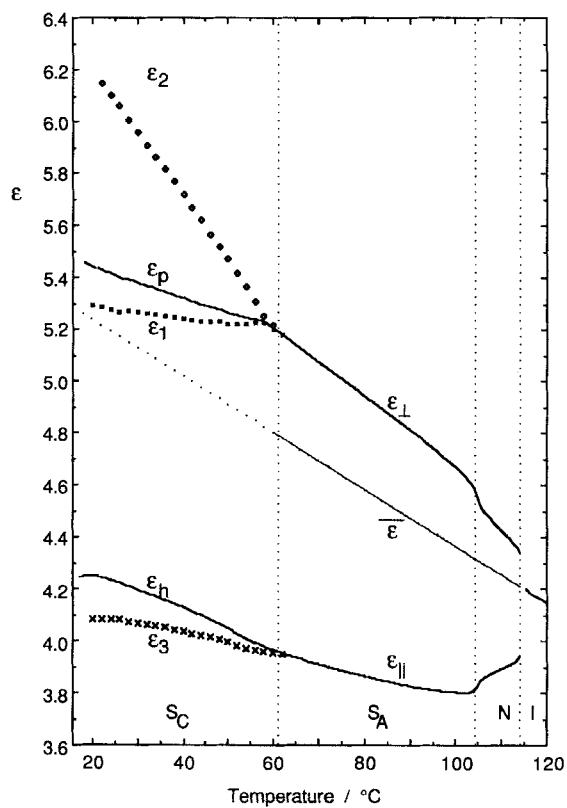

Figure 10. Temperature dependence of the permittivities for the racemic DiFTP mixture M1.
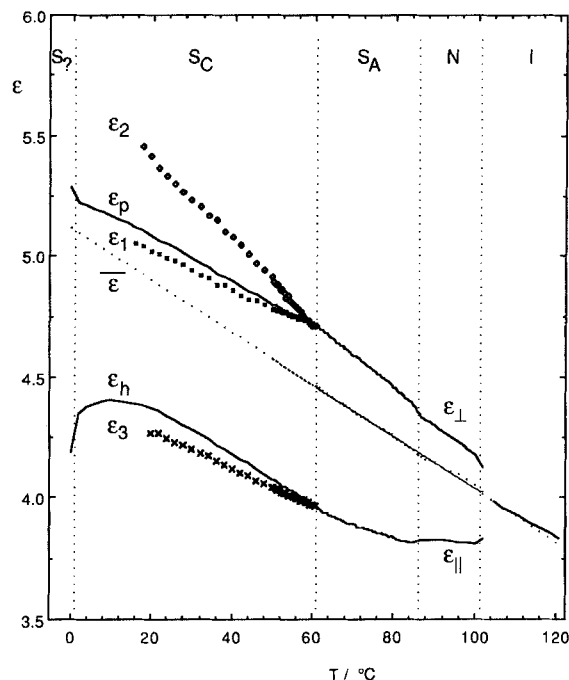
Figure 11. Temperature dependence of the permittivities for the racemic commercial ferroelectric liquid crystal mixture SCE13(R).

Table 4. Summary of the S_C permittivities at $T_{S_C S_A} - T = 30°C$ for several host mixtures.

	Host	$T_{S_C S_A}/°C$	ε_1 ($\pm 1\%$)	$\Delta\varepsilon$ (± 0.06)	$\partial\varepsilon$ (± 0.1)
H1	RRMBF	73.3	3.842	−0.61	+0.26
H2	RORMBF	107.3	3.938	−0.73	+0.48
H3	PYP	55.0	2.894	+0.50	+0.10
H4	FTP	66.8	3.134	+0.08	+0.13
H5	DiFTP	91.5	4.624	−1.55	+0.76
M1	DiFTP	62.0	5.141	−1.07	+0.76
SCE13(R)	BDH	60.8	4.756	−1.03	+0.30

4. Sources of experimental error

Both types of cell were defect free when cooled slowly into the S_A phase from the nematic and an uncertainty in the permittivity of 0.25 per cent was assumed from repeated measurements. Any systematic error associated with the smectic alignment is likely to effect the linearity of the $\bar{\varepsilon}$ temperature dependence, and most of the materials studied were linear across the isotropic, nematic and smectic A phases (see figures 5 to 11). A drop in $\bar{\varepsilon}$ was observed for the pyrimidine host H3, (see figure 7), although good smectic alignment was observed for both homeotropic and planar homogenous cells. This type of behaviour also occurred in other pyrimidine mixtures and is typical of materials with anti-parallel dipole correlations associated with smectic ordering [26]. There was no evidence for dipole correlations in any of the other materials studied.

In the S_C phase, the permittivity of the planar homogenous geometry ε_p includes the effect of domain walls and any defects, such as the characteristic zig-zag. The experimental uncertainty is correspondingly difficult to estimate, but repeated measurements have suggested that it is better than 0·3 per cent for samples with the most uniform S_C textures. The main sources of error for the calculated S_C permittivities $\varepsilon_1, \varepsilon_2$ and ε_3 determined using the method described in § 3, are due to uncertainty in θ, δ and the extrapolated values of $\bar{\varepsilon}$. Each of these factors leads to an uncertainty which is related to the temperature below the S_A to S_C phase transition $T_{S_C S_A}$. Except within about 2°C of the transition temperature, the experimental uncertainties are dominated by the accuracy of the $\bar{\varepsilon}$ extrapolation. For most of the materials used the following temperature dependences for the experimental uncertainties were estimated

$$\%_0\varepsilon_1 = \pm(0\cdot02(T_{S_C S_A} - T) + 0\cdot3)\%$$

$$\%_0\varepsilon_2 = \pm(0\cdot08(T_{S_C S_A} - T) + 0\cdot3)\%$$

$$\%_0\varepsilon_3 = \pm(0\cdot005(T_{S_C S_A} - T) + 0\cdot3)\%$$

For example, at $T_{S_C S_A} - T = 30°C$, the accuracies are approximately 1, 3 and 0·5 per cent for $\varepsilon_1, \varepsilon_2$ and ε_3, respectively. Slightly higher levels of uncertainty occurred with the PYP host H3 due to the poor linearity of the $\bar{\varepsilon}$ (T) curve. The short N and S_A temperature range of the MBF host H2 also leads to an increased uncertainty, but confidence in the $\bar{\varepsilon}$ extrapolation is increased because of the underlying uniaxial S_B phase.

Systematic errors will arise if the planar homogenous sample is not uniform. A uniform director profile would appear completely black when viewed between crossed polarizers and oriented at angle β_i. However, a slight coloration of the $S_C^{(*)}$ domains is usually observed, indicating that the director profile varies from one surface to the other. In this situation the permittivity is no longer described by equation (14), but has a complicated dependence on the director profile throughout the active volume. Assuming that the director profile only varies in the direction parallel to the measuring field and the chevron interface is at the cell centre, the generalized expression for the permittivity of a non-uniform state is

$$\frac{1}{\varepsilon} = \frac{1}{d}\left(\int_0^{d/2} \frac{1}{\varepsilon_{yy}}\,dy + \int_{d/2}^d \frac{1}{\varepsilon_{yy}}\,dy \right). \tag{17}$$

For director profiles with constant layer tilt δ and cone angle θ, and which are symmetric (or anti-symmetric) either side of the chevron interface the measured permittivity is

$$\frac{1}{\varepsilon} = \frac{2}{d}\int_0^d \frac{1}{\varepsilon_{yy}}\,dy$$

$$= \frac{2}{d}\int_0^d \frac{1}{A\sin^2\varphi + B\sin\varphi + C}\,dy, \tag{18}$$

where the constants A, B and C are

$$A = (\varepsilon_1\cos^2\theta - \varepsilon_2 + \varepsilon_3\sin^2\theta)\cos^2\delta,$$

$$B = \tfrac{1}{2}(\varepsilon_1 - \varepsilon_3)\sin 2\delta\sin 2\theta,$$

$$C = \varepsilon_2 + (\varepsilon_1\sin^2\theta - \varepsilon_2 + \varepsilon_3\cos^2\theta)\sin^2\delta.$$

The zero-field $S_C^{(*)}$ director profile is that which has the minimum elastic energy, given the constraints of the chevron layer structure and the cell boundaries. At the chevron interface, the director is required to lie parallel to the plane of the cell at the angle φ_i given by equation (11). The azimuthal angle at the surface φ_s is related to the anchoring energies associated with deviation of the director away from the preferred alignment direction and the surface plane, and the elastic distortion of the liquid crystal: for low surface pre-tilts $\varphi_i \leqslant \varphi_s \leqslant \pi/2$ is likely. Within these constraints, the simplest director profile is a linear variation from φ_s at one surface, to φ_i at the chevron interface and back to φ_s at the other surface [27]. If the layer tilt angle is close to the cone angle, the out-of-plane tilt throughout the sample is negligible, and the in-plane twist has a triangular director profile, shown in figure 1 (b). Optical studies [12] show that the triangular profile is a good approximation to the director profile in typical planar homogenous cells. The permittivity of a triangular profile sample is

$$\frac{1}{\varepsilon} = \frac{\displaystyle\int_{\varphi_s}^{\varphi_i} \frac{1}{\sin\varphi - \alpha}\,d\varphi - \int_{\varphi_s}^{\varphi_i} \frac{1}{\sin\varphi - \beta}\,d\varphi}{(\varphi_i - \varphi_s)\cos\delta\sqrt{[(\varepsilon_2 - \varepsilon_3)(\varepsilon_2 - \delta\varepsilon\sin^2\delta) + \varepsilon_2\Delta\varepsilon\cos^2\theta]}}, \tag{19}$$

where the roots α and β are

$$(\alpha, \beta) = \frac{\dfrac{\Delta\varepsilon}{2}\sin\delta\sin 2\theta \pm \sqrt{[(\varepsilon_2 - \varepsilon_3)(\varepsilon_2 - \delta\varepsilon\sin^2\delta) + \varepsilon_2\Delta\varepsilon\cos^2\theta]}}{(\Delta\varepsilon\sin^2\theta - \partial\varepsilon)\cos\delta}. \tag{20}$$

Equation (19) is solved using the standard solutions

$$\left.
\begin{aligned}
\int \frac{1}{\sin\varphi - \alpha}\,d\varphi &= \frac{2}{\sqrt{(\alpha^2 - 1)}}\tan^{-1}\left(\frac{1 - \alpha\tan(\varphi/2)}{\sqrt{(\alpha^2 - 1)}}\right); & \alpha^2 &> 1, \\[2ex]
\int \frac{1}{\sin\varphi - \alpha}\,d\varphi &= \frac{1}{\sqrt{(1 - \alpha^2)}}\log\left(\frac{1 - \alpha\tan(\varphi/2) - \sqrt{(1 - \alpha^2)}}{1 - \alpha\tan(\varphi/2) + \sqrt{(1 - \alpha^2)}}\right); & \alpha^2 &< 1.
\end{aligned}
\right\} \tag{21}$$

For example, well below the S_A–$S_C^{(*)}$ phase transition (i.e. θ and δ are large) and for typical permittivities

$$\varepsilon = \frac{(\varphi_m - \varphi_s)\cos\delta\sqrt{[(\varepsilon_2 - \varepsilon_3)(\varepsilon_2 - \delta\varepsilon\sin^2\delta) + \varepsilon_2\Delta\varepsilon\cos^2\theta]}}{\left[\dfrac{1}{\sqrt{(\alpha^2 - 1)}}\tan^{-1}\left(\dfrac{1 - \alpha\tan(\varphi/}{\sqrt{(\alpha^2 - 1)}}\right) - \dfrac{1}{\sqrt{(\beta^2 - 1)}}\tan^{-1}\left(\dfrac{1 - \beta\tan(\varphi/2)}{\sqrt{(\beta^2 - 1)}}\right)\right]_{\varphi_s}^{\varphi_i}}. \tag{22}$$

For samples with small surface pre-tilts, the largest systematic error associated with the triangular director profile occurs for $\varphi_s = \pi/2$. The temperature dependence of the M1 S_C permittivities calculated using equation (11) are compared with those calculated using equation (19) with $\varphi_s = \pi/2$ in figure 12. For example, ε_1 increases by 4 per cent and ε_2 decreases by 2 per cent at $T_{S_CS_A} - T = 30°C$. Clearly, the value of φ_s will depend on the liquid crystal and the surface alignment agent. Whereas the best fit of the optics of an S_C cell with polyimide alignment layers leads to $\varphi_s \approx \pi/2$ [12], the uniform director profile measured in [11] suggests that $\varphi_s \approx \varphi_i$ where 30° SiO alignment layers were used. Thus, we expect any systematic error in the calculated S_C permittivities due to the formation of a non-uniform director profile in the planar geometry to be negligible when 30° SiO cells are used to measure ε_p and conclude that the present results are satisfactory.
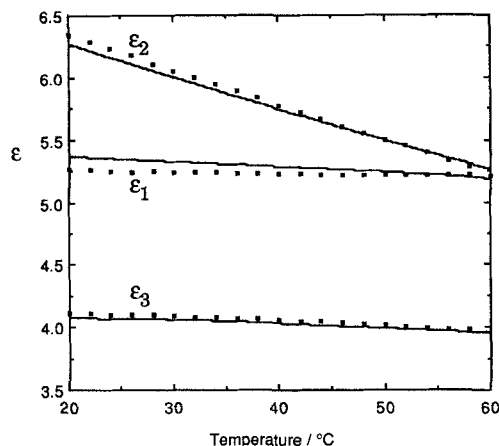
Figure 12.   Comparison of the S_C permittivities calculated assuming a chevron geometry for ε_p with a uniform director profile ($\cdot$) and a triangular director profile (—) for the DiFTP mixture M1.

5. Discussion

Application of an AC electric field across an S_C sample causes the director to move about the cone towards the orientation of minimum electrostatic energy, which occurs when the maximum permittivity component is parallel to the applied field. Assuming that field induced changes in the S_C cone angle and layer orientation are negligible, the director reorientation involves changes of azimuthal angle. Each of the present materials exhibits positive values of dielectric biaxiality $\partial\varepsilon$. Hence, application of an AC field couples to $\partial\varepsilon$, inducing the change in azimuthal angle from the surface stabilized state given by equation (11) towards the fully switched state $\varphi = n\pi$, and the extinction angle increases correspondingly from that predicted by equation (1) towards that of equation (9). This is the principle of AC field stabilization, which will only occur for materials with $\varepsilon_2 > \varepsilon_1$. Negative biaxial materials ($\varepsilon_2 < \varepsilon_1$) would exhibit decreasing extinction angle with applied AC field, but since this type of behaviour has not yet been observed, most materials must have positive dielectric biaxialities.

The applied field also causes an increase in the out-of-plane tilt from $\zeta = 0$ towards the switched state tilt angle ζ_s predicted by equation (10). The permittivity ε_{yy} then includes a contribution from the component parallel to the director ε_3. For negative materials (i.e. $\Delta\varepsilon < 0$), ε_3 is lower than the perpendicular permittivities and the electrostatic energy is a minimum at an azimuthal angle φ_∞

$$\sin\varphi_\infty = \frac{\tan\delta\cos\theta\sin\theta}{\sin^2\theta - (\partial\varepsilon/\Delta\varepsilon)},\tag{23}$$

which may be somewhat different from the fully switched state of $\varphi = n\pi$. This implies that, contrary to popular belief, a negative dielectric anisotropy is detrimental to the AC field effect, because the applied AC field does not stabilize the fully switched state but that given by equation (23). Substituting equation (23) into equation (7) allows the director twist angle (and the extinction angle if the director profile is uniform) for the AC field stabilized state to be calculated (see figure 13). Maximum efficacy of the AC stabilizing field occurs when the ratio ($\Delta\varepsilon/\partial\varepsilon$) is close to zero. Figure 13 also includes the results of table 4 and shows that the dielectric biaxiality is sufficiently large to cause a significant AC field stabilization for each of the present materials. This is because the
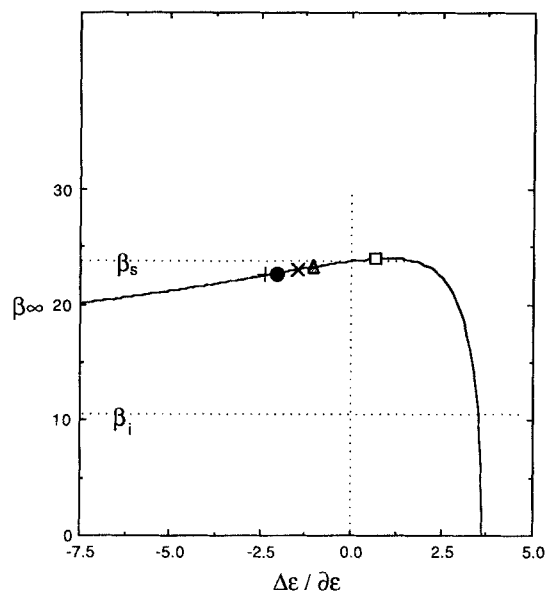
Figure 13. Theoretical prediction for the extinction angle at infinite AC field plotted as a function of $\Delta\varepsilon/\partial\varepsilon$ (for $\theta = 22\cdot5°$ and $\delta = 20°$). The points represent the value of $(\Delta\varepsilon/\partial\varepsilon)$ for each material at $T_{S_C S_A} - T = 30°C$ given in table 4. ($+$) H1 (MBFRR), ($\times$) H2 (MBF ROR), ($\square$) H4 (FTP), ($\bullet$) HF (DiFTP) and ($\triangle$)M1,SCE13.

transverse molecular dipole moment contributes to both a negative $\Delta\varepsilon$ and a positive $\partial\varepsilon$, such that all of the hosts have similar values of $(\Delta\varepsilon/\partial\varepsilon)$. This explains partly why the extinction angle for a given applied voltage and shifted temperature $(T_{S_C S_A} - T)$ is rather insensitive to the material used [28]. Material improvements may be envisaged, however, in which the molecular dipole μ contributes to $\partial\varepsilon$ without enhancing the negative $\Delta\varepsilon$, for example by making both the parallel $(\mu_\parallel)$ and perpendicular $(\mu_\perp)$ dipole components large.

Dielectric biaxiality not only drives AC field stabilization with the chevron layer structure, but will play an important role in all electric field behaviour of S_C and S_C^* devices. For example, the minimum response time of ferroelectric devices reported in [1] is due to the effect of the permittivities dominating the ferroelectric liquid crystal response time at high field strengths [1, 3]. The field at which the minimum response time occurs is related to both $\partial\varepsilon$ and $\Delta\varepsilon$ (as well as θ and δ) in a complicated manner, and this will be discussed in a forthcoming publication [29].

The present method used to determine the three $S_C^{(*)}$ permittivities relies on the assumption that the dielectric and optical cone angles are equivalent. To test this, a fourth dielectric measurement is required, either by choosing an appropriate director profile using a different surface alignment, or reorientation of the director through application of external fields. Either method requires defect-free alignment and a known director profile. Other geometries based on high surface pretilt alignments [30] may provide suitable, uniform director profiles. However, X-ray and optical studies are required before such geometries may be used to determine the permittivities. Alternatively, electric or magnetic field induced reorientation of the director will lead to a change in the measured permittivity providing additional information concerning the $S_C^{(*)}$ permittivities. Prediction of the director profile with an applied field requires a suitable continuum theory and for a given applied field the director profile will depend

on the relevant elastic constants and boundary conditions. Nematic permittivities may be determined by extrapolation to the fully switched state without knowledge of the elastic constants [31]. There are several problems associated with using external fields to determine $S_C^{(*)}$ permittivities. The director is not only constrained at the surfaces but also at the chevron interface and full switching of the director, therefore, is likely to involve some disruption of the chevron structure. For simplicity, it is common to describe the motion of the c-director in a nematic-like manner [32]. However, microscopic observations suggest that the $S_C^{(*)}$ does not deform continuously with applied field but induces defects [33] at higher field strengths, which are probably associated with reorientation of the smectic layers. Thus, measurements are restricted to lower field strengths, where the director remains unswitched at the surfaces and chevron interface.

6. Conclusion

An accurate method for measurement of S_C and S_C^* permittivities has been proposed, which is based on a more complete understanding of the director profiles in the measurement geometries than has previously been possible. The results for a series of host compounds and two racemic versions of ferroelectric liquid crystal mixtures suggest that the dielectric biaxiality is large, and cannot be ignored, agreeing with previous work [5], which confirmed that the electric field behaviour of achiral S_C systems can be dominated by dielectric biaxiality. Future descriptions of ferroelectric liquid crystal devices will need to incorporate all three biaxial permittivities to predict the electro-optic behaviour more realistically.

References

[1] ORIHARA, H., NAKAMURA, K., ISHIBASHI, Y., YAMADA, Y., YAMAMOTO, N., and YAMAWAKI, Y., 1986, *Jap. J. appl. Phys.*, 25, L839.

[2] HUGHES, J. R., and SAUNDERS, F. C., 1988, *RSRE Technical Memorandum 4139*.

[3] SAUNDERS, F. C., HUGHES, J. R., PEDLINGHAM, H. A., and TOWLER, M. J., 1989, *Liq. Crystals*, 6, 341.

[4] LEPESANT, J. P., PERBET, J. N., MOUREY, B., HARENG, M., DECOBERT, G., and DUBOIS, J. C., 1985, *Molec. Crystals liq. Crystals*, 129, 161.

[5] JONES, J. C., RAYNES, E. P., TOWLER, M. J., and SAMBLES, J. R., 1990, *Molec. Crystals liq. Crystals Lett.*, 7, 91.

[6] RIEKER, T. P., CLARK, N. A. SMITH, G. S., PARMAR, D. S., SIROTA, E. B., and SAFINYA, C. R., 1987, *Phys. Rev. Lett.*, 59, 2658.

[7] GAROFF, S., 1977, Ph.D. Thesis, Harvard University, Massachusetts, U.S.A.

[8] BENGUIGUI, L., and CABIB, D., 1978, *Phys. Stat. Sol. (a)*, 47, 71.

[9] HOFFMAN, J., KUCZYNSKI, W., MALECKI, J., and PAVEL, J., 1987, *Ferroelectrics*, 76, 61.

[10] GRAY, G. W., and GOODBY, J. W., 1984, *Smectic Liquid Crystals* (Leonard Hill).

[11] SAMBLES, J. R., ELSTON, S., and CLARK, M. G., 1989, *J. mod. Opt.*, 36, 1019.

[12] ANDERSON, M. H., JONES, J. C., RAYNES, E. P., and TOWLER, M. J., 1991, *J. Phys. D*, 34, 338.

[13] DRUON, C., and WACRENIER, J. M., 1984, *Molec. Crystals liq. Crystals*, 108, 291.

[14] CLARK, N. A., RIEKER, T. P., and MACLENNAN, J. E., 1988, *Ferroelectrics*, 85, 79.

[15] DE GENNES, P. G., 1974, *The Physics of Liquid Crystals* (Clarendon Press).

[16] MACLENNAN, J. E., CLARK, N. A., HANDSCHY, M. A., and MEADOWS, M. R., 1990, *Liq. Crystals*, 7, 753.

[17] BISHOP, D. I., JENNER, J., and SAGE, I., 1986, *11th International Liquid Crystal Conference*, Berkeley, U.S.A.

[18] ZASCHKE, H., 1975, *J. P. Chem.*, **317**, 617.
[19] CHAN, L. K. M., GRAY, G. W., and LACEY, D., 1985, *Molec. Crystals. liq. Crystals*, **40**, 33.
[20] GRAY, G. W., HIRD, M., LACEY, D., and TOYNE, K. J., 1989, *J. chem. Soc. Perkin Trans.*, **2**, 2041.
[21] BRADSHAW, M. J., BRIMMELL, V., CONSTANT, J., HUGHES, J. R., RAYNES, E. P., SAMRA, A. K., CHAN, L. K. M., GRAY, G. W., LACEY, D., SCROWSTON, R. M., SHENOUDA, I. G., TOYNE, K. J., JENNER, J. A., and SAGE, I. C., 1988, *Proceedings of the SID*, **29**, 3, 245.
[22] BRADSHAW, M. J., 1984, Ph.D. Thesis, University of Exeter, U.K.
[23] JONES, J. C., and RAYNES, E. P. (to be published).
[24] JONES, J. C., RAYNES, E. P., TOWLER, M. J., and SAMBLES, J. R., 1989, *British Liquid Crystal Society Annual Conference*, Sheffield, U.K.
[25] ELSTON, S. J., SAMBLES, J. R., and CLARK, M. G., 1990, *J. appl. Phys*, **68**, 1242.
[26] DE JEU, W. H., 1980, *Physical Properties of Liquid Crystalline Materials* (Gordon & Breach).
[27] JONES, J. C., 1991, Ph.D. Thesis, The University of Hull, U.K.
[28] MINTER, V. (unpublished work).
[29] TOWLER, M. J., JONES, J. C., and RAYNES, E. P., *Liq. Crystals* (to be published).
[30] RIEKER, T. P., CLARK, N. A., SMITH, G. S., and SAFINYA, C. R., 1989, *Liq. Crystals*, **6**, 565.
[31] CLARK, M. G., RAYNES, E. P., SMITH, R. A. S., and TOUGH, R. J. A., 1980, *J. Phys. D*, **13**, 2151.
[32] HANDSCHY, M. A., and CLARK, N. A., 1984, *Ferroelectrics*, **59**, 69.
[33] SATO, Y., TANAKA, T., NAGATA, M., TAKESHITA, H., and MOROZUMI, S., 1987, *Proceedings of the SID*, **28**, 189.